IEEE Access
Multidisciplinary ⋮ Rapid Review ⋮ Open Access Journal

Received February 13, 2022, accepted February 22, 2022, date of publication February 28, 2022, date of current version March 8, 2022.

Digital Object Identifier 10.1109/ACCESS.2022.3155234

Design and Analysis of a Novel Compact Metamaterial Absorber Based on Double-Layer ITO Resistive Film for Improving Signal Integrity

XIAOYONG LEI[1], YAN LI[2], (Senior Member, IEEE), SHUYUN HUO[1], ZHE SUN[1], HEYUAN YU[1], LIDAN FANG[2], SHAOJIE XU[2], BINGHENG LI[3], MENGJUN WANG[1], AND ERPING LI[1,2,3], (Fellow, IEEE)

[1]School of Electronics and Information Engineering, Hebei University of Technology, Tianjin 300401, China
[2]Key Laboratory of Electromagnetic Wave Information Technology and Metrology of Zhejiang Province, College of Information Engineering, China Jiliang University, Hangzhou 310018, China
[3]Zhejiang Provincial Key Laboratory of Advanced Microelectronic Intelligent Systems and Applications, School of Information and Electronic Engineering, Zhejiang University, Hangzhou 310027, China

Corresponding author: Yan Li (liyan@cjlu.edu.cn)

This work was supported by the Natural Science Foundation of China under Grant 62071424 and Grant 62027805.

ABSTRACT This paper presents a compact metamaterial absorber (MMA) based on double-layer ITO resistive film for suppression of electromagnetic interference (EMI) to improve signal quality and signal integrity (SI). In the design of MMA, based on the classic Jerusalem cross, circular and fan-shaped structures are combined to increase its equivalent capacitance to achieve frequency shift, and an equivalent circuit model is established to analyze the key factors affecting its absorption rate. At the same time, the full-wave simulation results show that more than 90% absorption rate is achieved in the frequency range of 8.9 GHz-14.0 GHz, and the measurement results show that the absorption rate of MMA at different incident angles is consistent with the simulation. Moreover, microstrip antenna and differential microstrip transmission line are also designed as equivalent radiation sources. The co-simulation results show that the 3 m field radiation of the patch antenna is reduced by 10 $dB\mu V$ at 10 GHz. At the same time, the eye height of the differential microstrip transmission line has increased from 68 mV to 340 mV, indicating that the signal integrity problem has been significantly improved. The size of the unit is only about 0.065 $\lambda_L \times 0.065\ \lambda_L$ where λ_L is the wavelength of the lowest frequency, and the total thickness of the absorber is only 0.047 λ_L. The proposed MMA has the characteristics of miniaturization, ultra-wideband, high absorption rate, and polarization insensitivity, which provides a new suppression method for the radiation problem of gradually miniaturized electronic equipment.

INDEX TERMS Miniaturized, ITO resistive film, metamaterial absorber (MMA), signal integrity (SI), electromagnetic interference suppression.

I. INTRODUCTION

The advent of 5G has led higher operating frequencies and integration levels of existing electronic equipment, and EMI problems become increasingly serious [1]. In order to solve such problems, reflection and absorption schemes are generally used for radiation suppression [2]. The reflection suppression scheme is relatively simple. For example, radiation suppression can be achieved by sputtering and electroplating a thin metal layer of less than 10 μm on a single package unit with radiation exceeding the standard. However, on the one hand, the cost of this method is very high, on the other hand, electromagnetic waves reflected inside the package will cause electromagnetic immunity problems and affect the quality of signal transmission [3]. However, another solution can effectively absorb the incident electromagnetic wave, and there will be neither transmission nor reflection in the working frequency band, and it is easier to ameliorate SI [4]–[7].

The associate editor coordinating the review of this manuscript and approving it for publication was Mohamed Kheir.

MMA is widely used because of its small thickness, high absorption rate and adjustable resonance frequency. In 2008, Landy *et al*. designed a perfect metamaterial absorber for the first time, and the electromagnetic characteristics were adjusted by changing the size of the surface structure to achieve perfect matching with free space impedance and achieve high absorption rate [8]. However, the early MMA unit has a narrow bandwidth, a large size, and depends on the incident angle and polarization direction of electromagnetic waves. Therefore, many researchers have proposed different design schemes for such problem. A large number of studies have found that loading lumped elements (capacitors, inductors, and resistors) are the most direct and effective way to expand bandwidth, mainly because the introduction of lumped elements makes it easier to achieve impedance matching and convert the incident electromagnetic energy absorption into heat [9]–[13]. However, the MMA unit cell structure cannot be miniaturized due to the size limitations of the lumped element itself. With the deepening of the research, the mainstream bandwidth expansion methods have been proposed, including stacked and spoof surface plasmon polaritons to confine the incident electromagnetic wave to the surface and then consuming them. However, the above method are limited by the thickness and complex material, resulting in difficulties in practical application [14]–[19]. At the same time, in the actual complex electromagnetic environment, not only the bandwidth needs to be considered, but polarization-sensitive and incident angle stability are also the key considerations. When the angle of incident electromagnetic wave increases, impedance mismatch and central frequency shift will occur. Most researchers use central symmetric structure to avoid polarization sensitivity at the beginning of design. The miniaturization of MMA also improves the angle stability. Therefore, the design of an ultra-wideband polarization insensitive absorber which is easy to realize miniaturization has become a research hotspot [20]. In this paper, a high absorption rate MMA with the size of 2.2 mm × 2.2 mm × 1.6 mm for the X and Ku waveband is proposed. The MMA structure consists of a Jerusalem cross printed on glass and a fan-shaped ITO conductive film. The backplane uses ITO with a surface resistance of 5 Ω/sq instead of all metal copper to realize a double-layer ITO resistive film. The thickness of the substrate is 0.047 λ_L, which breaks through the requirement (1/4 λ) of the traditional absorber. At the same time, the patch antenna and transmission line are designed as radiation sources to verify the influence of MMA on electromagnetic radiation and signal integrity.

The rest of this article is organized as follows. Section II presents the design of the MMA unit structure and analyzes the factors affecting the absorption performance of the absorber. In Section III, the absorbing mechanism of MMA is introduced through the extraction of the equivalent electromagnetic parameters. At the same time, the application of MMA in improving SI is introduced. The corresponding patch antenna is designed as the radiation source and the absorption rate of MMA is verified through experiments in Section IV. Finally, a brief conclusion is given in Section V.

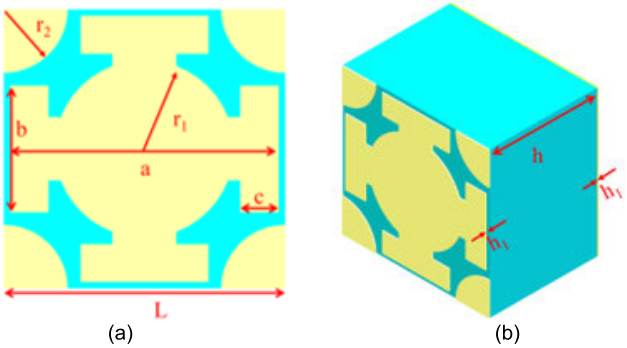

FIGURE 1. Total MMA structure design, (a) Front view, (b) 3D view.

II. DESIGN AND SIMULATION OF MMA

A. DESCRIPTION OF MMA UNITS

The MMA is printed on the dielectric substrate in a periodic array pattern to achieve impedance matching with free space impedance. When the electromagnetic wave is incident on the surface of the medium, part of the energy is reflected and transmitted, the rest of the energy is absorbed. According to the law of energy conservation, the absorptivity is calculated as:

$$A(\omega) = 1 - R(\omega) - T(\omega), \tag{1}$$

where $R(\omega)$ and $T(\omega)$ denote reflectance and transmissivity respectively, $R(\omega) = |S_{11}|^2$ and $T(\omega) = |S_{21}|^2$.

Since the backplate of the absorber is all metal, which leads to the transmission coefficient $T(\omega) = 0$, the calculation equation of the absorptivity is rewritten as:

$$A(\omega) = 1 - R(\omega) = 1 - |S_{11}|^2 . \tag{2}$$

Figure.1 shows the structure of the MMA unit. The parameter values of the absorber are shown in Table 1. The periodic unit is composed of three parts: the ITO resistive film on the top layer, the substrate in the middle layer and the ITO resistive film on the bottom layer. The top layer resistance film on the increases its equivalent capacitance and inductance by increasing the circular and fan-shaped structures, which causes the resonance point to move to a low frequency. In order to illustrate the design principle more clearly, based on the equivalent circuit theory, the structure of the MMA is replaced by circuit analog. The change of impedance is used to characterize the transmission characteristics of incident electromagnetic wave in the MMA. As shown in Figure 2, Z_0 is the free space impedance, Z_{in} is the input impedance, Z_{h} is the dielectric impedance. The structure of the top layer resistive film is equivalent to an *RLC* series circuit, where *R*, *L* and *C* respectively represent the equivalent resistance, inductance and capacitance of the top part of the MMA.

According to the transmission line theory, the input impedance Z_{in} of the absorber is equivalent to the parallel value of the dielectric impedance Z_{h} and the surface

TABLE 1. Geometries of the MMA (Unit: MM).

r_1	r_2	a	b	c	h	h_1	L
0.7	0.5	2.1	1.0	0.3	1.6	23nm	2.2

impedance Z_p, which can be retrieved from the equivalent circuit diagram using the following equation:

$$Z_P = R + j\omega L - 1/(j\omega C), \tag{3}$$

where, R is related to the sheet resistivity R_f of the top resistive film, can be approximately obtained as,

$$R = \frac{S_1}{S_2} R_f, \tag{4}$$

where S_1 is the area of the unit structure, S_2 is the area of the resistive film. Using transmission line theory, Z_{in} can be expressed as:

$$Z_{in} = \frac{1}{1/Z_p + 1/Z_h} = \frac{Z_p \times Z_h}{Z_p + Z_h}. \tag{5}$$

The dielectric impedance Z_h from the absorber can be calculated as:

$$Z_h = Z_{re} + \mathrm{j}Z_0 \sqrt{\frac{1}{\varepsilon_r}} \tan\left(\omega h \sqrt{\varepsilon_0 \varepsilon_r \mu_0}\right), \tag{6}$$

where, ε_0 is the vacuum permittivity, μ_0 is the vacuum permeability, Z_{re} represents the impedance corresponding to the lossy grounding plane, ε_r is the relative permittivity of the medium, ω is the resonant angular frequency, h is the thickness of the medium.

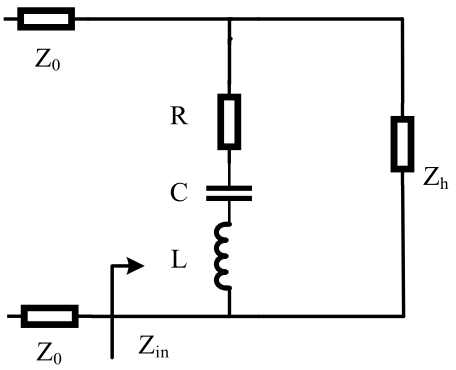

FIGURE 2. Equivalent circuit.

The equivalent inductance L of the MMA is mainly composed of the mutual inductance of the resistive film between the top and bottom layers and the self-inductance inside the top resistive film structure. Since the structure pattern has been determined, it is considered that the L is a fixed value. The equivalent capacitance C is also composed of two parts, including the capacitance C_1 between the top and bottom resistive films and the gap capacitance C_2 between the top resistive film structure. Considering that the electric field resonance of the absorber is dominant, and the electric field component of electromagnetic radiation is mainly distributed in the gap, it can be considered that the equivalent capacitance C is approximately equal to C_2. Therefore, C can be expressed as:

$$C \approx C_2 \propto \varepsilon_r / l, \tag{7}$$

where l is the gap size between the top-level unit structure. When other parameters remain unchanged, C is only related to and proportional to the permittivity of the medium. When impedance matching is achieved, the MMA will generate electromagnetic resonance, and the resonance frequency can be expressed as [21]:

$$f = \frac{\omega}{2\pi} = \frac{c}{4h\sqrt{\varepsilon_r}}. \tag{8}$$

In summary, the permittivity ε_r and thickness h of the medium and the sheet resistivity R_f of the surface resistive film are the key parameters that affect the MMA, and the perfect absorber can be achieved through proper adjustment.

B. INFLUENCING FACTORS OF ABSORPTION RATE

According to the above theory, the full-wave simulator, CST Microwave Studio is employed to simulate MMA in frequency-domain, and the boundary conditions is set as ''unit cell'' in the X and Y directions and ''open add space'' in the Z direction. First, the influence of medium thickness on the absorbing performance is explored. Keep other variables remain unchanged and the thickness of the medium increases in the range of 1.4 mm-1.7 mm to obtain S_{11} of the absorber. According to equation (8), the resonant frequency of the MMA is inversely proportional to the thickness of the medium, and the increase of the thickness of the medium will lead to the shift of the resonant frequency to the low frequency when other conditions remain unchanged. At the same time, according to equation (6), the increase in thickness will also lead to an increase in Z_h. Once Z_h increases, Z_{in} will inevitably increase. When h is the optimal value, the input impedance is equal to the free space impedance, the reflection coefficient tends to 0, and the absorption rate tends to 100%. When the thickness continues to increase, it will inevitably lead to impedance mismatch, which leads to a decrease in the resonance depth and a decrease in the absorption rate. The simulation results in Figure 3(a) are consistent with the theoretical derivation. Therefore, thickness is one of the key parameters affecting the MMA, and the impedance matching is realized when $h = 1.6$ mm.

Similarly, it is necessary to further study the influence of the permittivity ε_r on the S parameter. In general, the real part of the ε_r is two orders of magnitude larger than the imaginary part. Therefore, the influence of the change of the real part of the dielectric constant on the absorbing performance is mainly discussed here. Set the dielectric constant of the medium as a variable and increase it from 4.5 to 7.5 at intervals of 1. It can be seen from Figure 3(b) that as the permittivity ε_r increases, the resonant frequency shifts to low frequency and the absorption rate increases. When the permittivity is 6.5, the resonance depth of 10 GHz is -57dB.

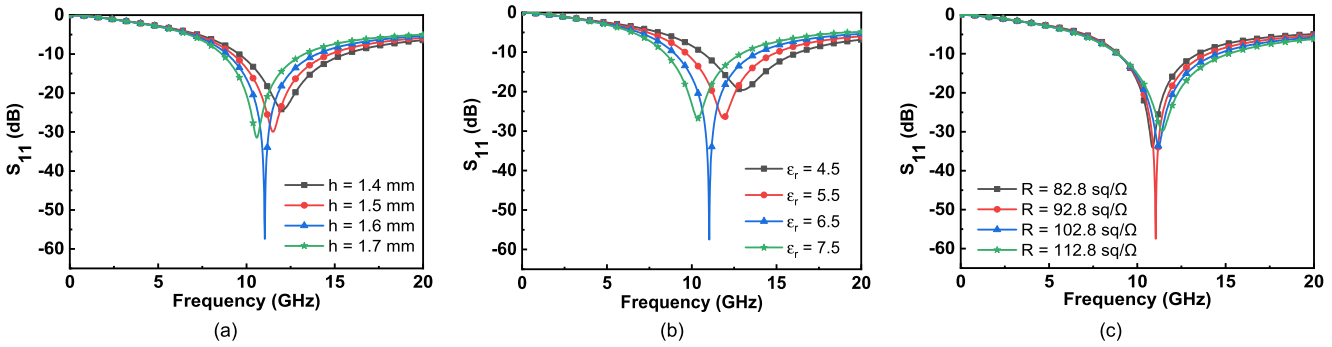

FIGURE 3. The influence of key parameters on S-parameters, (a) Change of dielectric thickness, (b) Change of dielectric constant, (c) Change of resistance film square resistance.

When the ε_r continues to increase, the resonance frequency continues to shift to low frequencies and the absorption rate decreases. According to the equivalent circuit analysis, the dielectric constant is inversely proportional to the square of the resonant frequency. As the dielectric constant increases, the resonant frequency continuous to shift to low frequencies. In addition, according to equations (3) and (7), with the increase of dielectric constant, the equivalent capacitance increases, resulting in the increase of input impedance. Similarly, when the dielectric constant is at the optimal value, the input impedance and freedom are realized. Therefore, when the $\varepsilon_r = 6.5$, the input impedance matches the free space impedance, thus confirming that the ε_r is one of the important parameters that affect the absorption rate of the MMA.

The surface resistance of the MMA is very high. In order to study the influence of the sheet resistivity of the resistive film on the S parameter, the resistance value $\boldsymbol{R}$ is set as a variable for simulation analysis without changing other conditions. According to the equivalent circuit theory, R will not change the resonant frequency, but will affect the surface impedance to control impedance matching. As shown in Figure 3(c), the simulation results are consistent with the theoretical analysis. When $\boldsymbol{R = 92.8\,\Omega/sq}$, the input impedance can be matched with the free space impedance.

Of course, sometimes when the above three conditions are determined, the frequency offset and impedance matching can also be achieved by changing the resistive film structure of the top layer. As shown in Figure 4, when circular and fan-shaped patches are added to the traditional Jerusalem cross, the equivalent inductance and capacitance are increased. According to the equivalent circuit, the resonance frequency is shifted to low frequencies and the surface impedance is increased, which makes the input impedance faster to achieve impedance matching, i.e., the absorption rate increases.

C. NUMERICAL SIMULATION

After determining the value of each parameter of the structure, the absorption rate is analyzed by CST simulation. The absorption rate curve is calculated by (2). As shown in Figure 5, the red curve represents the S_{11} parameter, the

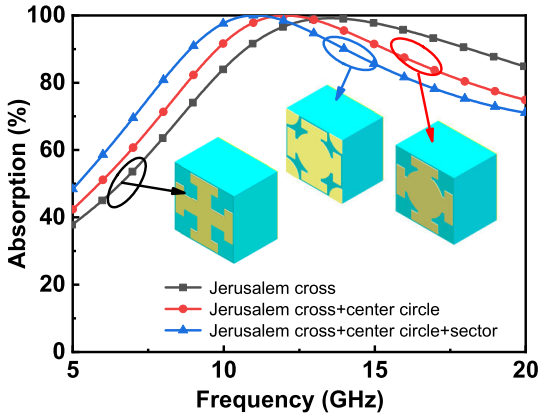

FIGURE 4. The effect of top structure changes on the absorption rate.

resonance depth reaches -57dB, and the black curve represents the calculated absorption rate. The absorption rate of more than 90% is achieved at 8.9 GHz-14.0 GHz, the relative bandwidth reaches 44.5% to achieve ultra-wideband.

When the electromagnetic environment is complex, the polarization angle and incident angle are the key factors that affect the absorption performance of MMA. Due to the central symmetry of the structure itself, it has polarization-insensitive characteristics. As shown in Figure 6 (a) and (b), when the polarization angle changes in the range of 0°-90°, the absorption rate in TE and TM polarization modes remains unchanged, which proves that the structure is insensitive to polarization.

In order to ensure the angle stability, the structure of the MMA is simulated by the oblique incident. Figure 7(a) and (b) show the relationship curves of absorption rate affected by different incident angles in TE and TM polarization modes, respectively. When the incident angle of the electromagnetic wave is in the range of 0°-40°, the absorption rate of the absorber in the working frequency band is always higher than 90%. With the increase of the incident angle, the absorption rate gradually decreases. When the incident angle is 60°, the absorption rate and bandwidth of the TE mode are significantly reduced, but the absorption rate is still more than 80% in the frequency range of 9.4 GHz-12.8 GHz. However, the absorption bandwidth increases in TM mode

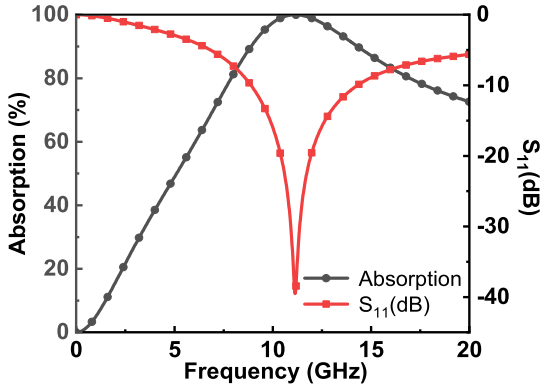

FIGURE 5. S parameter and absorptivity under normal incidence.

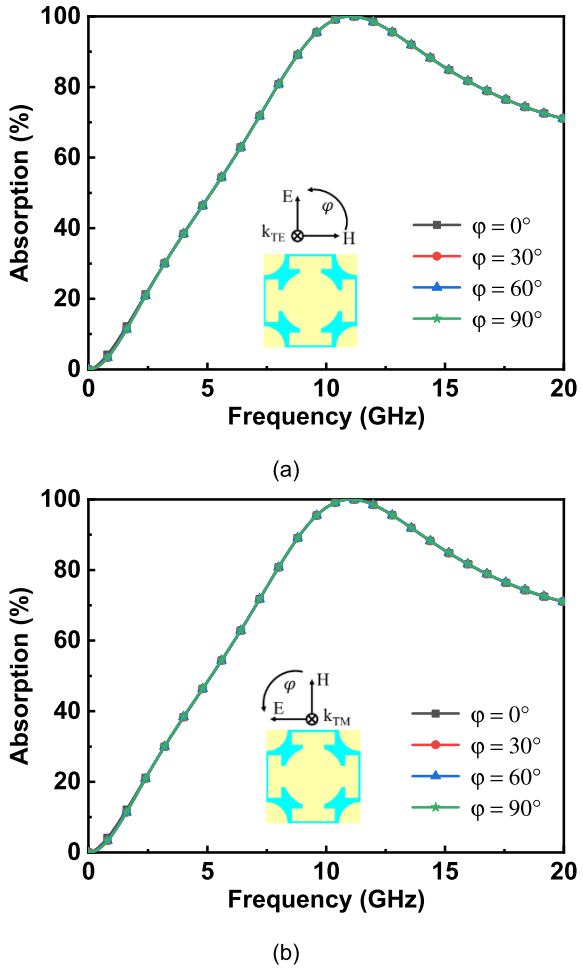

FIGURE 6. Absorption rate under different polarization angles in different polarization modes, (a) TE polarization, (b) TM polarization.

and the absorption rates after 8 GHz is higher than 80%, so the structure has good angular stability.

III. ABSORPTION MECHANISM

A. EQUIVALENT ELECTROMAGNETIC PARAMETER ANALYSIS

In order to verify the absorbing mechanism of MMA, the surface electric field and current were analyzed in detail by CST

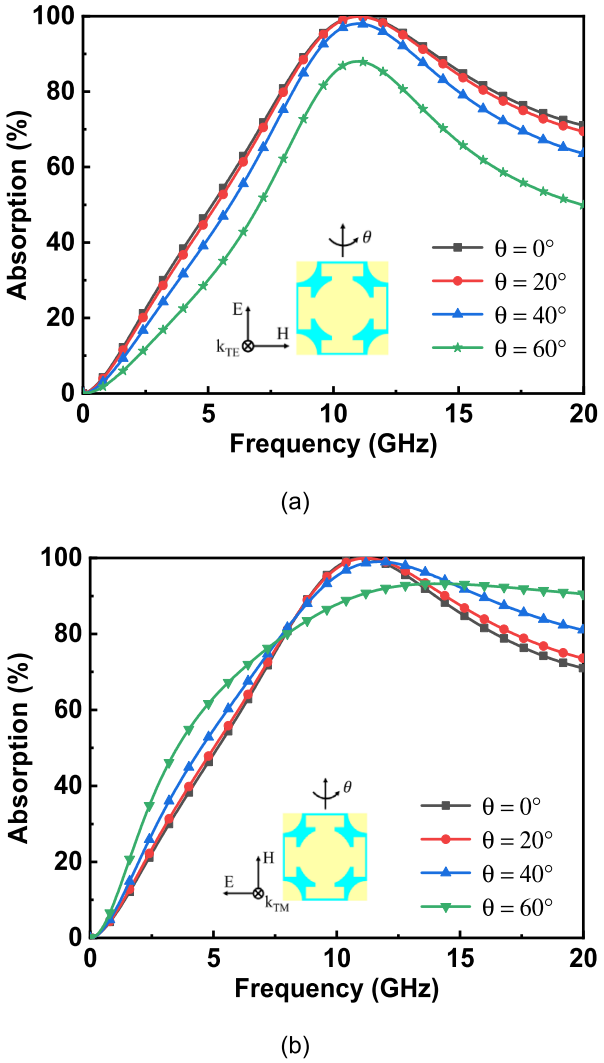

FIGURE 7. Absorption rate at different incident angles in different polarization modes, (a) TE polarization, (b) TM polarization.

simulation software. The surface current and the electric field distributions of the proposed MMA at the resonant frequency, i.e., 11 GHz, are shown in Figure 8. Figure 8(a) and (b) show the surface current of the top and bottom layer of the MMA at 11 GHz. As shown in Figure 8(a), the current on the top layer generates an equivalent capacitance through the gap between the central symmetrical structure and the side sector, forming a current loop, exciting the electric dipole and causing electrical resonance, thereby controlling the permittivity $\varepsilon(\omega)$. As shown in Figure 8(b), the current on the bottom surface is opposite to the corresponding top surface current. The upper and lower sides form a circulating current loop, which excites the magnetic dipole and causes magnetic resonance to control the permeability $\mu(\omega)$. Figure 8(c) is the electric field distribution at 11 GHz. It can be seen from the color that the color at the edges and gaps is the reddest, and the electric field radiation is the strongest. This further shows that the top resistive film structure will produce strong electrical resonance and change the permittivity $\varepsilon(\omega)$. Therefore, the impedance

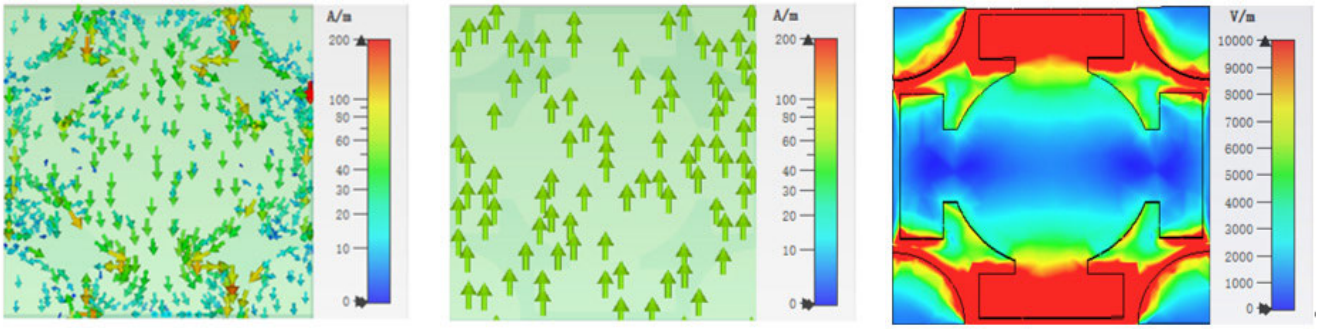

(a) (b) (c)

FIGURE 8. Distribution of surface current and electric field, (a) top surface current at 11 GHz, (b) bottom surface current at 11 GHz, (c) surface electric field at 11 GHz.

matching between the incident wave and the free space can be achieved through the common adjustment of electromagnetic resonance, to achieve the purpose of broadband and high absorption. Not only that, the equivalent medium theory is one of the commonly used methods to analyze the absorption mechanism of MMA. Since the backplane is fully coated with ITO resistive film and has $S_{21} = 0$, the equivalent impedance can be written as follows [22]:

$$z(\omega) = \sqrt{\frac{(1+S_{11})^2 - S_{21}^2}{(1-S_{11})^2 - S_{21}^2}} = \frac{1+S_{11}}{1-S_{11}}, \tag{9}$$

$$S_{11} = \frac{z(\omega)-1}{z(\omega)+1}, \tag{10}$$

where $z(\omega)$ is the equivalent impedance of the MMA.

According to equation (2), the high absorptivity can be achieved when S_{11} is close to 0. Therefore, in the design of the absorber, and $z(\omega) = 1$ should be ensured as much as possible.

Because the backplane of the MMA is made of an ITO resistive film with a specific surface impedance, the attenuation of electromagnetic waves is very high and it is difficult to transmit. For a sufficiently large plane, the scattering is ignored, and the incident electromagnetic waves are absorbed except reflection. For this reason, a simple program is written to calculate the real and imaginary parts of the equivalent impedance using the S-parameter inversion method. As shown in Figure 9(a), the black curve and red curve represent the real and imaginary parts of the equivalent impedance respectively. It can be seen that in the range of 8.9 GHz-14.0 GHz, the black curve is close to 1, and the red curve is close to 0, which realized the impedance matching with the free space. Since $z(\omega) \neq 1$, the absorption rate cannot reach 100% and can only be infinitely close.

In addition, the constitutive parameters are also one of the important means to verify the absorbing mechanism of MMA. As mentioned above, the backplane of our MMA is equivalent to all copper-clad, so the equivalent medium theory is no longer applicable. The new calculation equations for equivalent dielectric constant $\varepsilon(\omega)$ and permeability $\mu(\omega)$ are as follows [23]:

$$\varepsilon(\omega) = 1 + \frac{2j}{k_0 h}\left(\frac{1-S_{11}}{1+S_{11}}\right), \tag{11}$$

$$\mu(\omega) = 1 + \frac{2j}{k_0 h}\left(\frac{1+S_{11}}{1-S_{11}}\right), \tag{12}$$

where k_0 is the free space wave number, h is the thickness of the substrate.

Figure 9(b) and (c) show the equivalent permittivity and permeability of the absorber, respectively. where the black curve and red curve represent the real and imaginary parts, respectively. The comparison results show that the working bandwidth is basically the same, the real part of the $\varepsilon(\omega)$ and $\mu(\omega)$ is close to 0, and the impedance matching with the free space is realized. The imaginary part of the equivalent electromagnetic parameter represents the loss of the absorbing body to the incident electromagnetic wave, and the imaginary part is all greater than 0 in 8.9 GHz-14.0 GHz, showing obvious absorption loss.

The loss of absorbers is generally divided into dielectric and ohmic loss. Figure 6(a) shows the absorption rate curve of the MMA glass substrate (lossy and loss-free). In order to see the trend of the two curves clearly, the red and blue dashed lines are used to indicate lossy and loss-free respectively. The results show that the two curves have the same trend, and the absorption rate in the range of 8.9 GHz-14.0 GHz is higher than 90%. Therefore, the loss of the glass substrate of the absorber has no effect on the absorptivity, and there is no dielectric loss. In order to further verify whether there is the ohmic loss in the top structure, figure 6(b) is obtained by comparing different materials, i.e., resistive film and PEC. The two curves in the figure are very different. The introduction of the resistive film makes the absorption rate of the structure much higher than that of traditional metal materials. Therefore, the MMA belongs to the ohmic loss type. In short, the loss type of MMA is not single, including dielectric loss and magnetic resonance loss, and ohmic loss is the main loss in this study. This means that the change in the permittivity of the dielectric material will not have a certain effect on the absorption rate. Therefore, several materials with different

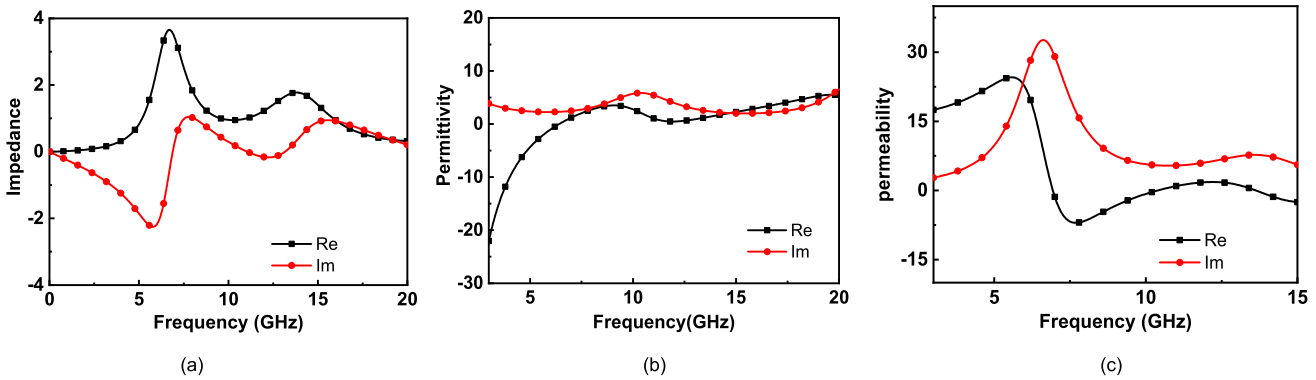

FIGURE 9. Equivalent parameters of MMA. (a) Equivalent impedance. (b) Equivalent permittivity. (c) Equivalent permeability.

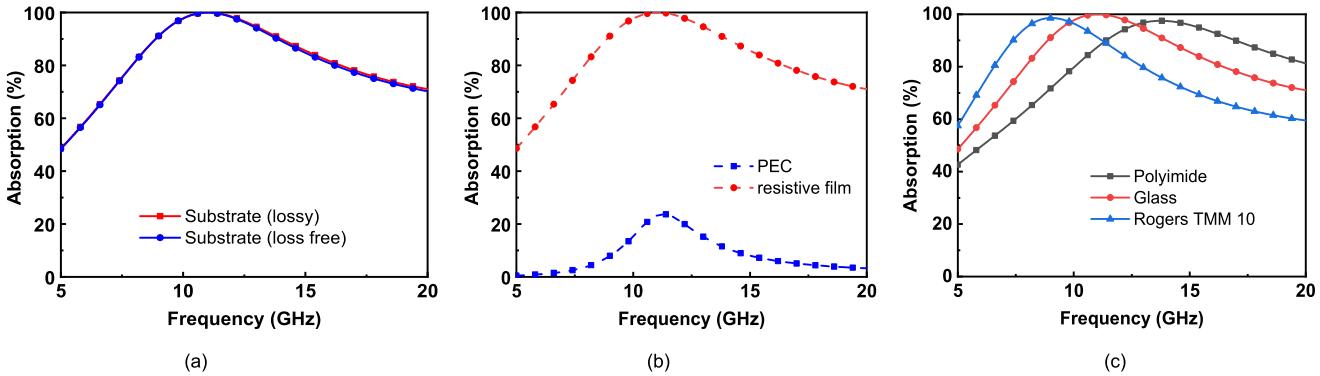

FIGURE 10. The effect of material property changes on the absorption rate. (a) Absorption rate of glass with or without loss. (b) Absorption rate under different top layer materials. (c) Absorption rate under different substrate materials.

TABLE 2. Simulation results of different dielectric substrates.

Substrate material	Permittivity	Bandwidth (GHz)	Relative bandwidth (%)
Polyimide	3.5	11.4-17.0	39.4
Glass	6.5	8.9-14.0	44.5
Rogers TMM 10	9.8	7.4-11.2	40.9

permittivity were simulated and analyzed to verify the above conjecture. Since the permittivity of the glass itself is 6.5, in order to ensure the reliability of the simulation results, two different materials with permittivity higher than 6.5 and lower than 6.5 are selected respectively, i.e., Rogers TMM 10 and Polyimide. Figure 6(c) shows the absorption rate curves of these three different materials, while Table 2 shows the material name, permittivity, working frequency band, and relative bandwidth. The results show that the change of the dielectric constant has little effect on the absorption rate. According to equation (8), as the permittivity of the substrate increases, the overall absorption frequency band shifts to low frequencies, and the absorption rate is not affected. Therefore, the high permittivity dielectric substrate is beneficial to the miniaturization of the MMA.

B. EQUIVALENT CIRCUIT ANALYSIS

In order to better analyze the absorbing principle of the metamaterial absorber, construct its equivalent circuit, as shown in Figure 11. Different from Figure 2, the parameters of the top-level structure are analyzed in detail, and the overall structure is divided into two parts, the fan shape and the Jerusalem cross. Therefore, R_1 and L_1 respectively represent the equivalent resistance and inductance of the Jerusalem cross in the center of the model, and C_{g1} represents the equivalent capacitance between the edge part and other unit structures. In addition, R_2 and L_2 represent the equivalent resistance and inductance of the surrounding sector structure, and C_{g2} represents the equivalent capacitance between the sector portion and the central structure. As determined in the previous analysis, the necessary condition for achieving high absorption is that the real part of the equivalent impedance is equal to 1 and the imaginary part is equal to 0, i.e., the real part of the input impedance is equal to the free space impedance and the imaginary part is equal to 0. The bottom plate of the absorber and the dielectric layer can be regarded as a terminal transmission line of length h, and the input admittance Y_{in} of the absorber is the

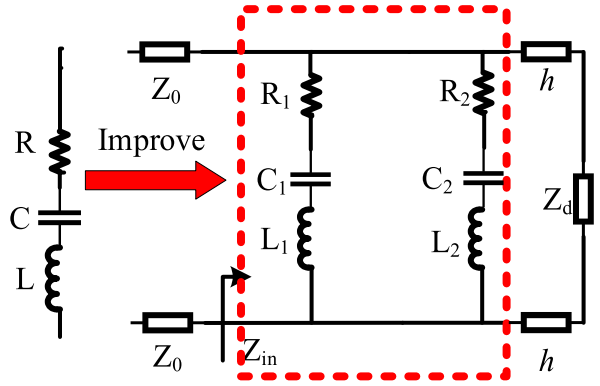

FIGURE 11. Detailed equivalent circuit.

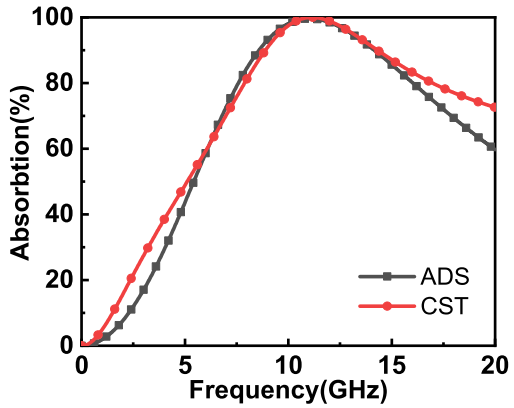

FIGURE 12. Comparison diagram of equivalent circuit simulation.

accumulation of the admittance values of each layer. Z_d represents ground loss. Therefore, the relationship between capacitance, inductance and resistance when perfect absorbing is obtained:

$$\frac{\omega^2 R_1 C_{g1}^2}{\left(1-\omega^2 L_1 C_{g1}\right)^2+\omega^2 R_1^2 C_{g1}^2}+\frac{\omega^2 R_2 C_{g2}^2}{\left(1-\omega^2 L_2 C_{g2}\right)^2+\omega^2 R_2^2 C_{g2}^2}=\frac{1}{Z_0} \tag{13}$$

$$\frac{\omega C_{g1}-\omega^3 L_1 C_{g1}^2}{\left(1-\omega^2 L_1 C_{g1}\right)^2+\omega^2 R_1^2 C_{g1}^2}+\frac{\omega C_{g2}-\omega^3 L_2 C_{g2}^2}{\left(1-\omega^2 L_2 C_{g2}\right)^2+\omega^2 R_2^2 C_{g2}^2}+\frac{\sqrt{\varepsilon_r}}{Z_0}\times\cot\left(\frac{2\pi f\sqrt{\varepsilon_r}h}{c}\right)=0 \tag{14}$$

where c represents the speed of light in free space, other parameters have been explained in the second section. Through ADS extraction and calculation, the parameter values of absorber lumped element are as follows: $R_1 = 152.8\ \Omega$, $R_2 = 572.2\ \Omega$, $L_1 = 15.4\ nH$, $L_2 = 12.4\ nH$, $C_{g1} = 20.7\ fF$, $C_{g2} = 11.3\ fF$. As shown in Figure 12, the S parameters obtained in ADS are converted into absorptivity, and compared with the simulation results of CST, the two curves basically coincide.

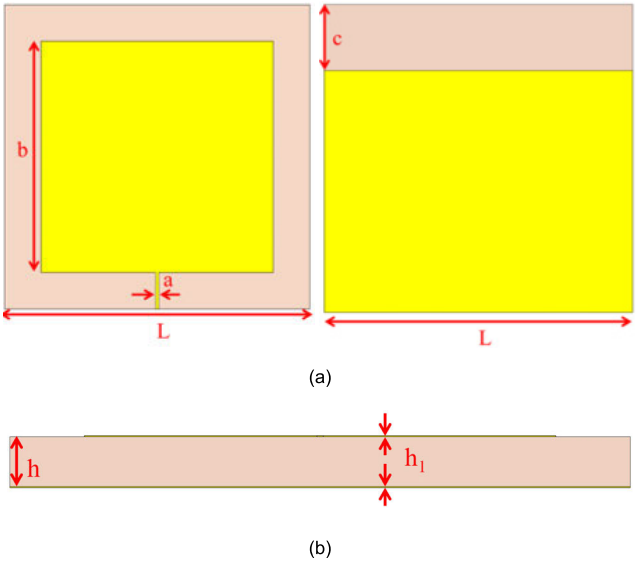

FIGURE 13. Three views of the microstrip patch antenna, (a) front side, (b) back side, (c) side view.

TABLE 3. Geometries of the microstrip antenna (Unit: MM).

a	*b*	*c*	*L*	*h*	h_1
0.2	*15.2*	*4.3*	*20*	*1.6*	*0.035*

C. RADIATION SUPPRESSION AND SI ANALYSIS

Because the ITO absorber has the characteristics of miniaturization, it can be used for chip level radiation suppression. At present, most of the radiation in the chip comes from inter board resonance, so the MMA can be placed under the heat sink in the form of array, and the top structure is facing the PCB. Suppress the radiation before it leaks into the space, so as to block the radiation path. Due to the chip model is confidential, we designed a microstrip antenna working at 10 GHz instead. As shown in Figure 13, the antenna is composed of a top metal patch, an intermediate dielectric layer, and a slotted metal ground plane at the bottom. The purpose of the slotted antenna is to excite the current and increase a certain bandwidth, making it easier to generate the operating frequency of 10 GHz for replacing the chip. The dielectric substrate adopts FR4, and the overall size is 20 mm × 20 mm × 1.6 mm, the width of the feeder port is 0.2 mm, the upper end of the ground plane of the backplane is slotted 4.3 mm. The parameter values of the microstrip antenna are shown in Table 3.

CST Microwave Studio is employed to simulate microstrip antenna in time-domain, and the boundary conditions is set as "open add space" in the X, Y and Z direction. Figure 14 shows the S parameters of the microstrip antenna. The resonance frequency is 10 GHz, which means that there will be a radiation peak near 10 GHz. As shown in Figure 15, the resistive film absorbing structure is placed 1mm above the antenna. And the closer the distance, the more obvious the suppression effect. Figure 16 shows the 1 m

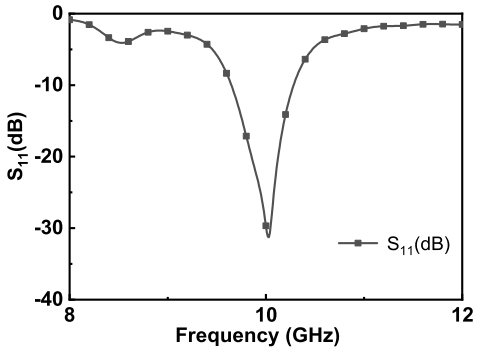

FIGURE 14. S parameter of patch antenna.

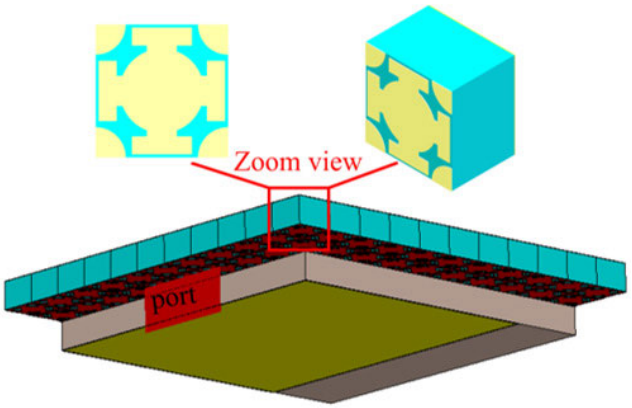

FIGURE 15. Arrangement of resistive film structure.

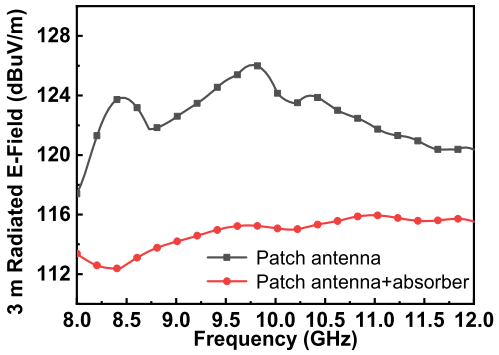

FIGURE 16. 3 m far field result comparison chart.

far-field result after loading the absorbing structure. It has obvious suppression effect in the range of 8 GHz-12 GHz, and the radiated energy at 10 GHz is reduced by 10 $dB\mu V$. Since there is the slot on the back of the microstrip antenna, there is a certain radiation leakage, which reduces a certain suppression effect, but the purpose of radiation suppression can be generally achieved. In the same way, it is equally effective when applied to the radiation suppression of miniaturized electronic equipment. Compared with traditional suppression schemes, resistive film absorbers can expand the suppression bandwidth, miniaturize the design structure, and maximize the suppression of specific frequency points.

In order to further verify the influence of the metamaterial absorber on the signal integrity, the corresponding transmission line structure needs to be designed. Therefore, in order

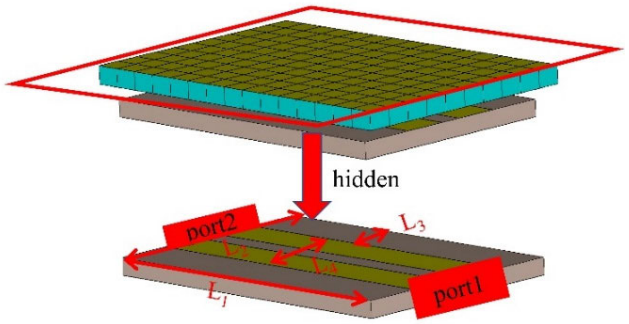

FIGURE 17. Differential microstrip transmission line.

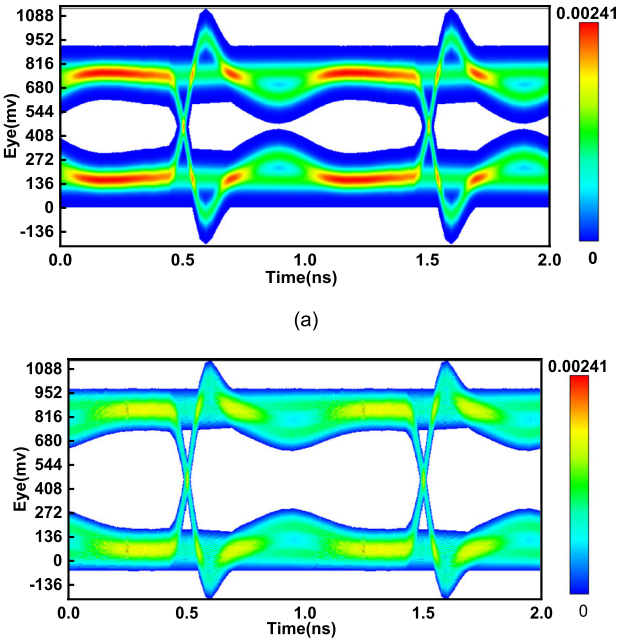

FIGURE 18. The eye diagram of the transmission line, (a) without MMA structure, (b) MMA structure in use.

to simplify the design, the thickness and material of the base are the same as that of the antenna, with specific parameters $L_1 = 30$ mm, $L_2 = 20$ mm, $L_3 = 5$ mm and $L_4 = 10$ mm, as shown in Figure 17. The red diamond-shaped frame in the figure is the metamaterial absorber structure. The co-simulation model is similar to the antenna loading method, and the structure is tiled on the top layer with the strongest radiation. In order to intuitively obtain the influence of the MMA structure on the signal transmission capability, the eye diagram is an indispensable indicator. First, use the CST simulation software to set the step signal to generate the excitation source at port 1, and the total simulation time is 200 ns. Immediately, set the eye diagram tool through the obtained transient response, and observe the signal quality of port 2. As shown in Figure 18(a), the eye diagram of the differential microstrip transmission line is obtained, and the eye height is only 68 mV. The metamaterial absorber does not reduce the radiation of the microstrip differential line itself,

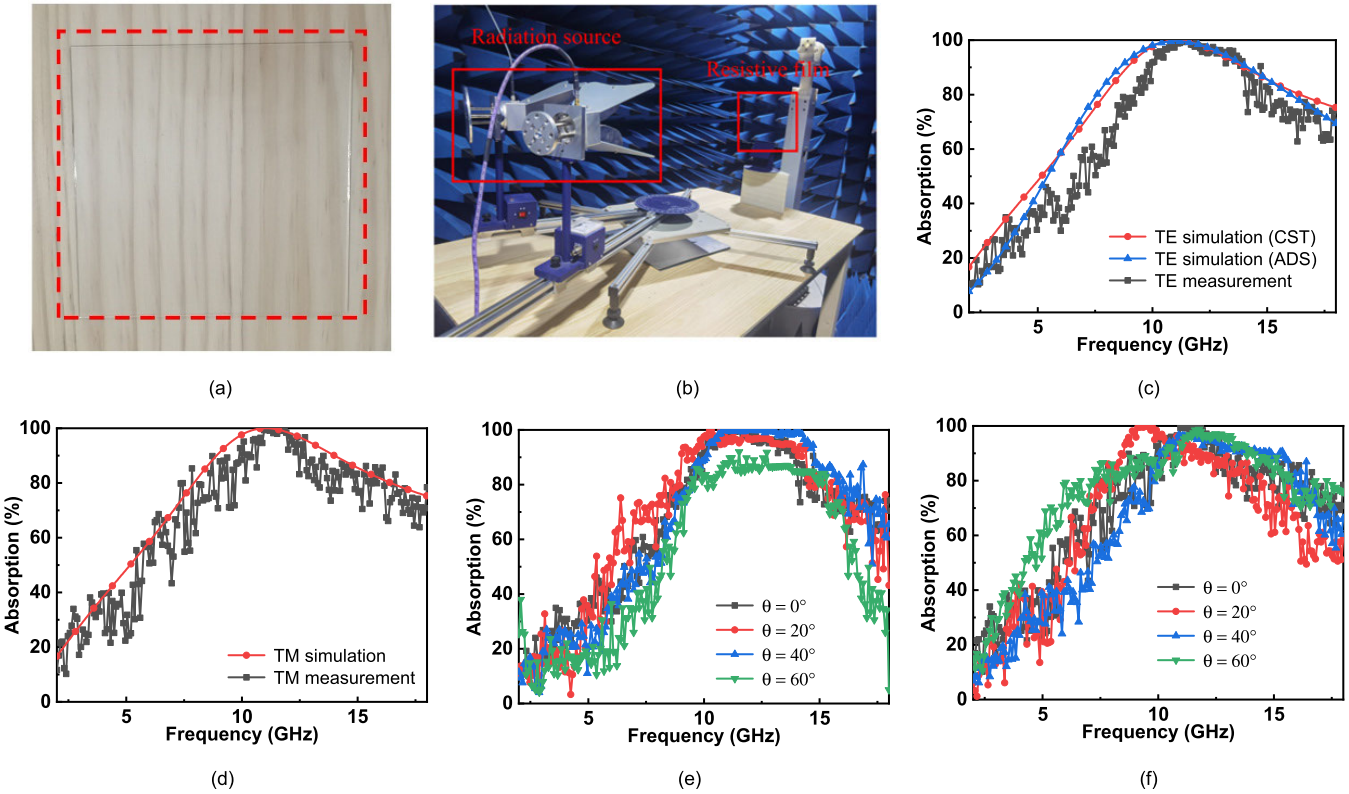

FIGURE 19. Measurement environment and results of absorption rates under different polarization modes, (a) MMA base on ITO resistive film, (b) Measured environment, (c) TE polarization, (d) TM polarization, (e) Different incident angles under TE polarization, (f) Different incident angles under TM polarization.

it is intended to cut off the radiation leakage problem in the propagation path. This results in very little radiation transmission to the terminal, so the eye chart of the receiving end will be improved and the eye height will increase significantly. As shown in Figure 18(b), the eyes diagram is obviously opened and the eye height is 340 mV, which proves that MMA will improve the signal integrity to a certain extent.

IV. ANALYSIS OF MEASUREMENT RESULTS

After gaining an in-depth understanding of the absorption characteristics of the resistive film absorber through theory and simulation, subsequent processing and measurement are carried out to further verify the absorption performance of the absorber. In order to facilitate the measurement, a glass substrate with a double-layer ITO resistive film is used. The top layer is laser-engraved to make an 80×80 array absorber structure. The bottom layer is an ITO film with a surface resistance of 5 Ω/sq. The overall size reaches 17.6 cm $\times$ 17.6 cm. Due to the glass substrate, the transparency of the absorber is very high, as shown in Figure 19(a), you can clearly see the texture of the wood on the back. As shown in Figure 19(b), fix to one side of the microwave anechoic chamber, and at the same time, two broadband double-ridged horn antennas operating at 1 GHz-18 GHz are required as the transmitter and receiver of electromagnetic waves, and they are placed side by side to face the absorber, keeping the same horizontal plane. Connect the two horn antennas to the Agilent N5244A vector network analyzer, and ensure that the far-field conditions between the MMA and the horn antenna are satisfied. The distance between the antenna and the MMA is much greater than $2L^2/\lambda_L$ (L represents the maximum diameter of the horn).

In order to verify the absorption rate of the absorber in different polarization modes, the directions of the two double-ridged horn antennas were rotated at 0° and 90° at the same time, and the S parameters of the TE and TM polarization modes were measured at normal incidence. According to equation (2) obtain the absorption rate curve. The absorptivity measurement result in TE and TM polarization modes are shown in Figures 19(c) and (d). Comparing the simulation and measurement results, the trend of the curve is basically the same, and there is an absorption peak near 11 GHz. Because the processing accuracy and environmental interference errors in the measurement are inevitable, the measured curve obtained is not smooth and there is noise interference, but the overall absorption bandwidth of the resistive film absorber is similar to the simulation, which further verifies the absorption performance of the absorber.

At the same time, in order to verify the angular stability of the absorbing body, the angle of the absorbing structure is rotated to measure the absorption rate when electromagnetic

TABLE 4. Comparison of developed MMA with relevant other papers.

Ref. #	Thickness	Unit Size	Bandwidth (GHz)	Relative Bandwidth (%)	Incidence Angle Sensitivity (°)
[24]	$0.057\lambda_L$	$0.229\lambda_L$	8.50 - 16.00	61.2	30
[25]	$0.122\lambda_L$	$0.234\lambda_L$	2.70 - 8.20	100.9	40
[26]	$0.092\lambda_L$	$0.141\lambda_L$	2.11 - 3.89	59.3	50
[27]	$0.611\lambda_L$	$0.140\lambda_L$	11.44 - 20.00	54.5	50
[28]	$0.073\lambda_L$	$0.377\lambda_L$	6.80 - 11.80	53.8	30
[29]	$0.067\lambda_L$	$0.260\lambda_L$	8.00 - 18.00	76.9	40
[30]	$0.138\lambda_L$	$0.172\lambda_L$	4.30 - 11.10	88.3	60
[31]	$0.030\lambda_L$	$0.283\lambda_L$	8.43 - 10.38	20.7	45
This work	$0.047\lambda_L$	$0.065\lambda_L$	8.90 - 14.00	44.5	60

waves are incident in the range of 0°-60°. As shown in Figure 19(e) and (f), with the increase of the incident angle, the absorption rate of the absorber decreases significantly, and the absorption bandwidth decreases in TE polarization mode, while increases in TM polarization mode, which is generally consistent with the simulation results. However, when the incident angle is 20°, the measurement result of the absorptance is shifted. The main reason is that when the angle of incidence is 20°, the measurement structure is tilted, which causes a certain change in the distance when the electromagnetic wave enters the absorber, thus causing the frequency to occur Certain offset.

The performance of this designed resistive film absorber was compared with some relevant works, as shown in Table 4. If the application is considered, the electromagnetic wave with an incident angle of 60° will not be affected by the reduction in bandwidth and absorptance at all, so I mark the incident angle as 60° in Table 4. Compared with other researches, the proposed absorber has miniaturization and a stable incidence angle. Although the relative bandwidth is only 44.5%, it also achieves ultra-wideband and has a high absorption rate in the X-band.

V. CONCLUSION

In this paper, a new type of the metamaterial absorber based on double layer ITO resistive film is designed to solve the radiation problem at chip package level and improve signal integrity. Full-wave simulations and measurement were carried out for validation of the structure. The structure realizes the polarization insensitivity due to the central symmetry and the result shows that the absorptivity is higher than 90% in the range of 8.9 GHz – 14.0 GHz when the electromagnetic wave is incident vertically. Additionally, the absorption rate of 10.0 GHz is still higher than 80% when the electromagnetic wave incident angle is 60°. When the absorber structure is loaded on the differential microstrip line, the eye diagram is significantly improved, and the eye height is increased from 68 mV to 340 mV. When a microstrip antenna is used as a radiation source, the suppression effect of the MMA achieves 10 $dB\mu V$ at 10 GHz. The structure we designed is more compact and has stronger angular stability by comparing with the recent research in Table 4, which is suitable for electromagnetic interference problem of complex chip packaging.

ACKNOWLEDGMENT

The authors would like to thank all referees for their constructive comments and suggestions in improving the quality of this paper.

REFERENCES

[1] Y. Li, W. Cao, P. Zuo, Y. Li, Z. Gao, M. Wang, H. Zheng, and E.-P. Li, "Analysis of multilayer structure near- and far-field radiation by the coupled PP-PEEC and field-equivalence principle method," *IEEE Trans. Electromagn. Compat.*, vol. 61, no. 2, pp. 495–503, Apr. 2019.

[2] T. Li, D. Li, P. Qin, Y. Fan, Y. Gu, P. Zuo, W. E. I. Sha, and E. Li, "A novel miniaturized strong-coupled FSS structure with excellent angular stability," *IEEE Trans. Electromagn. Compat.*, vol. 63, no. 1, pp. 38–45, Feb. 2021.

[3] S. Erickson and M. Sakaguchi, "Application of package-level high-performance EMI shield material with a novel nozzleless spray coating technology," in *Proc. IEEE 70th Electron. Compon. Technol. Conf. (ECTC)*, Jun. 2020, pp. 1691–1696.

[4] S. Hannan, M. T. Islam, A. Hoque, M. J. Singh, and A. F. Almutairi, "Design of a novel double negative metamaterial absorber atom for Ku and K band applications," *Electronics*, vol. 8, no. 8, p. 853, Jul. 2019.

[5] F. Venneri, S. Costanzo, and A. A. Borgia, "A dual-band compact metamaterial absorber with fractal geometry," *Electronics*, vol. 8, no. 8, p. 879, 2019.

[6] M. Edries, H. A. Mohamed, S. S. Hekal, M. A. El-Morsy, and H. A. Mansour, "A new compact quad-band metamaterial absorber using interlaced I/square resonators: Design, fabrication, and characterization," *IEEE Access*, vol. 8, pp. 143723–143733, 2020.

[7] S. Kalraiya, M. Ameen, R. K. Chaudhary, and R. K. Gangwar, "Compact ultrathin conformal metamaterial dual-band absorber for curved surfaces," *Int. J. RF Microw. Comput.-Aided Eng.*, vol. 29, no. 12, Dec. 2019, Art. no. e21929.

[8] N. I. Landy, S. Sajuyigbe, J. J. Mock, D. R. Smith, and W. J. Padilla, "Perfect metamaterial absorber," *Phys. Rev. Lett.*, vol. 100, May 2008, Art. no. 207402.

[9] X. Wang and J. Wu, "Uncooled CMOS 2.5 THz detector comprising a metamaterial absorber loaded with resistors and a PTAT sensor," *Opt. Quantum Electron.*, vol. 53, no. 5, p. 217, May 2021.

[10] K. S. L. Al-badri, "Electromagnetic broad band absorber based on metamaterial and lumped resistance," *J. King Saud Univ. - Sci.*, vol. 32, no. 1, pp. 501–506, Jan. 2020.

[11] H. Jeong, T. T. Nguyen, and S. Lim, "Subwavelength metamaterial unit cell for low-frequency electromagnetic absorber applications," *Sci. Rep.*, vol. 8, no. 1, p. 16774, Dec. 2018.

[12] N. Bai, W. Xiang, J. Shen, C. Shen, and X. Sun, "A *Ka*-band folded waveguide traveling wave tube with lumped resistance metamaterial absorber," *IEEE Trans. Electron Devices*, vol. 67, no. 3, pp. 1248–1253, Mar. 2020.

[13] S. Kalraiya, R. K. Chaudhary, and M. A. Abdalla, "Design and analysis of polarization independent conformal wideband metamaterial absorber using resistor loaded sector shaped resonators," *J. Appl. Phys.*, vol. 125, no. 13, Apr. 2019, Art. no. 134904.

[14] L. Huang, D. R. Chowdhury, S. Ramani, and M. T. Reiten, "Experimental demonstration of terahertz metamaterial absorbers with a broad and flat high absorption band," *Opt. Lett.*, vol. 37, no. 2, pp. 154–156, 2012.

[15] C. Zhang, Q. Cheng, J. Yang, J. Zhao, and T. J. Cui, "Broadband metamaterial for optical transparency and microwave absorption," *Appl. Phys. Lett.*, vol. 110, no. 14, Apr. 2017, Art. no. 143511.
[16] Y. Zhang, Y. Li, Y. Cao, Y. Liu, and H. Zhang, "Graphene induced tunable and polarization-insensitive broadband metamaterial absorber," *Opt. Commun.*, vol. 382, no. 1, pp. 281–287, Jan. 2017.
[17] Y. Tayde, M. Saikia, K. V. Srivastava, and S. A. Ramakrishna, "Polarization-insensitive broadband multilayered absorber using screen printed patterns of resistive ink," *IEEE Antennas Wireless Propag. Lett.*, vol. 17, no. 12, pp. 2489–2493, Dec. 2018.
[18] T. Ji, Y. Wang, Y. Cui, Y. Lin, Y. Hao, and D. Li, "Flexible broadband plasmonic absorber on moth-eye substrate," *Mater. Today Energy*, vol. 5, pp. 181–186, Sep. 2017.
[19] Y. Fan, J. Wang, Y. Li, Y. Pang, L. Zheng, J. Xiang, J. Zhang, and S. Qu, "Ultra-thin and -broadband microwave magnetic absorber enhanced by phase gradient metasurface incorporation," *J. Phys. D, Appl. Phys.*, vol. 51, no. 21, May 2018, Art. no. 215001.
[20] M. D. Banadaki, A. A. Heidari, and M. Nakhkash, "A metamaterial absorber with a new compact unit cell," *IEEE Antennas Wireless Propag. Lett.*, vol. 17, no. 2, pp. 205–208, Feb. 2018.
[21] D. Sievenpiper, L. J. Zhang, R. F. J. Broas, N. G. Alexopolous, and E. Yablonovitch, "High-impedance electromagnetic surfaces with aforbidden frequency band," *IEEE Trans. Microw. Theory Techn.*, vol. 47, no. 11, pp. 2059–2074, Nov. 1999.
[22] D. R. Smith, S. Schultz, P. Markoš, and C. M. Soukoulis, "Determination of effective permittivity and permeability of metamaterials from reflection and transmission coefficients," *Phys. Rev. B, Condens. Matter*, vol. 65, no. 19, Apr. 2002, Art. no. 195104.
[23] C. L. Holloway, E. F. Kuester, J. A. Gordon, J. O'Hara, J. Booth, and D. R. Smith, "An overview of the theory and applications of metasurfaces: The two-dimensional equivalents of metamaterials," *IEEE Antenn. Propag. Mag.*, vol. 54, no. 4, pp. 10–35, Jul. 2012.
[24] A. Sharma, R. Panwar, and R. Khanna, "Experimental validation of a frequency-selective surface-loaded hybrid metamaterial absorber with wide bandwidth," *IEEE Magn. Lett.*, vol. 10, pp. 1–5, 2019.
[25] J. Yu and L. Liu, "A new nonexpandable surface mapping for the design of spherically conformal metamaterial absorbers," *Int. J. RF Microw. Comput.-Aided Eng.*, vol. 31, no. 1, pp. 1–8, Jan. 2021.
[26] Z. Zhang, L. Zhang, X. Chen, Z. Wu, Y. He, Y. Lv, and Y. Zou, "Broadband metamaterial absorber for low-frequency microwave absorption in the S-band and C-band," *J. Magn. Magn. Mater.*, vol. 497, Mar. 2020, Art. no. 166075.
[27] J. B. O. de Araújo, G. L. Siqueira, E. Kemptner, M. Weber, C. Junqueira, and M. M. Mosso, "An ultrathin and ultrawideband metamaterial absorber and an equivalent-circuit parameter retrieval method," *IEEE Trans. Antennas Propag.*, vol. 68, no. 5, pp. 3739–3746, May 2020.
[28] T. Q. H. Nguyen, T. K. T. Nguyen, T. N. Cao, H. Nguyen, and L. G. Bach, "Numerical study of a broadband metamaterial absorber using a single split circle ring and lumped resistors for X-band applications," *AIP Adv.*, vol. 10, no. 3, Mar. 2020, Art. no. 035326.
[29] T. K. T. Nguyen, T. N. Cao, N. H. Nguyen, L. D. Tuyen, X. K. Bui, C. L. Truong, D. L. Vu, and T. Q. H. Nguyen, "Simple design of a wideband and wide-angle insensitive metamaterial absorber using lumped resistors for X- and Ku-bands," *IEEE Photon. J.*, vol. 13, no. 3, pp. 1–10, Jun. 2021.
[30] H. Jiang, W. Yang, R. Li, S. Lei, B. Chen, H. Hu, and Z. Zhao, "A conformal metamaterial-based optically transparent microwave absorber with high angular stability," *IEEE Antennas Wireless Propag. Lett.*, vol. 20, no. 8, pp. 1399–1403, Aug. 2021.
[31] M. M. Tirkey and N. Gupta, "Broadband polarization-insensitive inkjet-printed conformal metamaterial absorber," *IEEE Trans. Electromagn. Compat.*, vol. 63, no. 6, pp. 1829–1836, Dec. 2021.

XIAOYONG LEI received the B.S. degree in communication engineering from the School of Electronic Engineering, Tianjin University of Technology and Education, Tianjin, China, in 2017. He is currently pursuing the M.S. degree in electronics and information engineering with the Hebei University of Technology, Tianjin.

His current research interests include metamaterial structural design and electromagnetic compatibility.

YAN LI (Senior Member, IEEE) received the Ph.D. degree in electrical engineering from the Hebei University of Technology, Tianjin, China, in 2019. From 2016 to 2019, she carried out her Ph.D. Research at Zhejiang University under the joint Ph.D. program. In September 2019, she joined China Jiliang University, Hangzhou, China, where she is currently an Assistant Professor with the College of Information Engineering. Her current research interests include signal integrity and power integrity of 3-D integrated circuits, fast and efficient computational electromagnetics, electromagnetic modeling and experiment method, and its application in high-speed electronics.

Dr. Li received an Outstanding Young Scientist Award at the Joint IEEE International Symposium on Electromagnetic Compatibility & Asia-Pacific Symposium on Electromagnetic Compatibility, Singapore, in 2018, the Best Student Paper Award at the IEEE International Symposium on Electromagnetic Compatibility, Xi'an, China, in 2017, the Outstanding Doctoral Graduate Award of Hebei Province, in 2019, and the Excellent Doctoral Dissertation Award of Hebei University of Technology, in 2020. She was the Secretary Chair and the Section Chair of the International Workshops on Electromagnetic Compatibility of Integrated Circuits (EMC COMPO), Haining, China, in 2019, the Section Chair of IEEE MTT-S International Conference on Numerical Electromagnetic and Multiphysics Modeling and Optimization (IEEE MTT-S NEMO), Hangzhou, in 2020, and the Section Chair of the 13th Global Symposium on Millimeter Waves &Terahertz (GSMM), Nanjing, China, in 2021.

SHUYUN HUO received the B.S. degree in communication engineering from the Shanghai Institute of Technology, Shanghai, China, in 2019. She is currently pursuing the M.S. degree in electronics and information engineering with the Hebei University of Technology, Tianjin, China.

Her current research interests include metamaterial absorber and integrated circuit EMC.

ZHE SUN received the B.S. degree from the School of Electronic Information and Automation, Tianjin University of Science and Technology, Tianjin, China, in 2020. He is currently pursuing the M.S. degree in electronics and information engineering with the Hebei University of Technology, Tianjin.

His current research interests include metamaterial structural design and electromagnetic compatibility.

HEYUAN YU received the B.S. degree from the College of Measurement and Control Technology and Communication Engineering, Harbin University of Science and Technology, Harbin, China, in 2019. He is currently pursuing the M.S. degree in electronics and information engineering with the Hebei University of Technology, Tianjin, China.

His current research interests include signal integrity and brain-like chips.

LIDAN FANG received the B.S. degree from the College of Communication Engineering, China Jiliang University College of Modern Science and Technology, Hangzhou, China, in 2020. She is currently pursuing the M.S. degree in electronic information engineering with China Jiliang University, Hangzhou.

Her current research interests include signal integrity and neuromorphic chips.

SHAOJIE XU received the B.S. degree in communication engineering from the College of Information Engineering, China Jiliang University, Hangzhou, China, in 2020, where he is currently pursuing the M.S. degree.

His current research interests include frequency selective surface, metamaterial, and electromagnetic compatibility.

BINGHENG LI received the B.S. degree in electronic engineering from the College of Information Science and Electronic Engineering, Zhejiang University, Hangzhou, China, in 2020, where he is currently pursuing the M.S. degree in electronic engineering.

His research interests include EMI issues on IC package and EMI source localization.

MENGJUN WANG was born in Hebei, China, in 1978. He received the B.S. degree in information engineering and the M.S. degree in physical electronics from the Hebei University of Technology, Tianjin, China, in 1999 and 2005, respectively, and the Ph.D. degree from Tianjin University, Tianjin, in 2008.

He is currently working as an Associate Professor with the School of Electronics and Information Engineering, Hebei University of Technology. His research interests include microwave radio frequency technology, flexible electronics devices, and electromagnetic compatibility.

ERPING LI (Fellow, IEEE) received the Ph.D. degree in electrical engineering from Sheffield Hallam University, Sheffield, U.K., in 1992.

In 2000, he joined the A*STAR Research Institute of High-Performance Computing, Singapore, as a Principal Scientist and the Director. Since 1989, he has been a Research Fellow, a Principal Research Engineer, an Associate Professor, and the Technical Director of the National University of Singapore. He is currently a Changjiang-Qianren Distinguished Professor with the Department of Information Science and Electronic Engineering, Zhejiang University, Hangzhou, China, the Dean of the Joint Institute of Zhejiang University—University of Illinois at Urbana–Champaign, Zhejiang University. He has been the general chair and the technical chair for many international conferences. He has been invited to give numerous invited talks and plenary speeches at various international conferences and forums. His current research interests include electrical modeling and design of micro/nanoscale integrated circuits, 3-D electronic package integration, and nanoplasmonic technology.

Prof. Li is a fellow of MIT Electromagnetics Academy, USA. He was a recipient of the 2015 IEEE Richard Stoddard Award on EMC, the IEEE EMC Technical Achievement Award, the Singapore IES Prestigious Engineering Achievement Award, the Changjiang Chair Professorship Award from the Ministry of Education in China, and a number of best paper awards. He was elected to the IEEE EMC Distinguished Lecturer, in 2007. He was the President of the 2006 International Zurich Symposium on EMC, the Founding General Chair of Asia-Pacific EMC Symposium, the General Chair for 2008, 2010, 2012, and 2016 APEMC, and 2010 IEEE Symposium on Electrical Design for Advanced Packaging Systems. From 2006 to 2008, he was an Associate Editor of the IEEE MICROWAVE AND WIRELESS COMPONENTS LETTERS, a Guest Editor of 2006 and 2010 IEEE TRANSACTIONS ON ELECTROMAGNETIC COMPATIBILITY Special Issues, and a Guest Editor of 2010 IEEE TRANSACTIONS ON MICROWAVE THEORY AND TECHNIQUES (MTT) Special Issue on APMC. He is currently an Associate Editor of the IEEE TRANSACTIONS ON ELECTROMAGNETIC COMPATIBILITY and IEEE TRANSACTIONS ON COMPONENTS, PACKAGING AND MANUFACTURING TECHNOLOGY. He is a Founding Member of the IEEE MTT-RF Nanotechnology Committee.